inorganics

MDPI

Review

Recent Progress on the Functionalization of Endohedral Metallofullerenes

Song Wang [1,2,*], Xianming Zhang [1], Xi Tan [2], Hongzhen Li [2], Songxin Dai [2], Bin Yao [2], Xingyan Liu [2], Youzhou He [2] and Fei Jin [3,*]

1 Engineering Research Center for Waste Oil Recovery Technology and Equipment, Ministry of Education, Chongqing Technology and Business University, Chongqing 400067, China; zxm215@126.com
2 Department of Materials Science and Engineering, College of Environment and Resources, Chongqing Technology and Business University, Chongqing 400067, China; 17843952097@163.com (X.T.); 2020412242@email.ctbu.edu.cn (H.L.); 19122079474@163.com (S.D.); yaobinpku@126.com (B.Y.); liuxingyan@ctbu.edu.cn (X.L.); yzhectbu@163.com (Y.H.)
3 Magnetism Key Laboratory of Zhejiang Province, China Jiliang University, Hangzhou 310018, China
* Correspondence: wangsong@ctbu.edu.cn (S.W.); jinfei@cjlu.edu.cn (F.J.)

Abstract: Functionalization of endohedral metallofullerenes (EMFs) plays an important role in exploring the reactivity of EMFs and stabilizing missing EMFs, thus conferring tunable properties and turning EMFs into applicable materials. In this review, we present exhaustive progress on the functionalization of EMFs since 2019. Classic functionalization reactions include Prato reactions, Bingel–Hirsch reactions, radical addition reactions, carbene addition reactions, and so on are summarized. And new complicated multi-component reactions and other creative reactions are presented as well. We also discuss the structural features of derivatives of EMFs and the corresponding reaction mechanisms to understand the reactivity and regioselectivity of EMFs. In the end, we make conclusions and put forward an outlook on the prospect of the functionalization of EMFs.

Keywords: endohedral metallofullerenes; functionalization; reactivity; regioselectivity; derivatives; DFT calculation

Citation: Wang, S.; Zhang, X.; Tan, X.; Li, H.; Dai, S.; Yao, B.; Liu, X.; He, Y.; Jin, F. Recent Progress on the Functionalization of Endohedral Metallofullerenes. *Inorganics* **2023**, *11*, 346. https://doi.org/10.3390/inorganics11080346

Academic Editors: Xing Lu, Filip Uhlík, Takeshi Akasaka and Zdenek Slanina

Received: 26 June 2023
Revised: 7 August 2023
Accepted: 16 August 2023
Published: 21 August 2023

1. Introduction

Endohedral metallofullerenes (EMFs) with the metallic atom(s) or cluster encapsulated inside the carbon cages exhibit unique molecular structure and physicochemical properties, conferring EMFs great potential application in biomedicine, optoelectronic, and spin devices [1,2].

Until now, hundreds of EMFs have been reported and it is found that metals from IA, IIA, IIIB, IVB, and VB groups can be entrapped in the carbon cage [1–3], especially Sc, Y, and lanthanides, and form various EMFs including conventional EMFs and cluster EMFs. In the past five years, Th- or U-based actinide EMFs become new family members, showing novel molecular structures [4–6].

Based on the entrapped metallic species, EMFs are usually divided into conventional EMFs including mono-metallofullerenes (e.g., $La@C_{82}$) [7], di-metallofullerenes (e.g., $La_2@C_{80}$) [7], tri-metallofullerenes (e.g., $Sm_3@C_{80}$) [8] and cluster metallofullerenes [2]. In 1999, $Sc_3N@C_{80}$, the first cluster metallofullerenes, was reported and also represented trimetallic nitride template (TNT) EMFs [9]. Later on, various cluster metallofullerenes such as carbides (e.g., $Sc_2C_2@C_{84}$ [10], $TiLu_2C@C_{80}$) [11], methano (e.g., $Sc_3CH@C_{80}$) [12], carbonitride (e.g., $Sc_3CN@C_{80}$) [13], oxide (e.g., $Sc_4O_2@C_{80}$) [14], sulfide (e.g., $Sc_2S@C_{82}$) [15] and cyano-clusters (e.g., $YCN@C_{82}$) [16] metallofullerenes have been successively reported. In particular, the embedded metallic species donates electrons (up to 6e) to the carbon cages [17,18], which significantly stabilizes EMFs and changes their electronic structures compared to that of pristine empty fullerenes.

EMFs show distinctive chemical properties compared to empty fullerenes due to the doping of embedded metallic species [1–3,19–21]. In 1995, Akasaka first reported the chemical reaction of La@C_{82} [22], which starts to tune the properties of EMFs. Up to now, various kinds of methods have been developed for the functionalization of EMFs including photochemical reactions [23,24], Diels−Alder reactions [25,26], Prato reactions [27,28], Bingel–Hirsch reactions [29,30], radical addition reactions [31,32] and so on [1–3]. The inherent properties of EMFs are investigated via functionalization, which is essential access to the application of EMFs. In addition, the functionalization of EMFs is beneficial to acquiring high-quality crystals of EMFs and characterizing the structures of EMFs by forming derivatives that reduce the symmetry of EMFs [33,34]. Hence, the functionalization of EMFs is a popular direction and lots of reviews on the functionalization of EMFs have been published [1–3,19,35].

In this review, we focus on recent progress in the functionalization of EMFs from 2019. Classic functionalization reactions of EMFs with variable endohedral specials, different cage sizes, and isomers are summarized. And new complicated multi-component reactions and other creative reactions are also presented. The structural features of derivatives of EMFs and the corresponding reaction mechanisms are mainly discussed to understand the reactivity and regioselectivity of EMFs. Finally, we make conclusions and put forward an outlook.

2. Functionalization Reactions

The functionalization of EMFs since 2019 was summarized in Table 1.

2.1. Silylation and Germylation

The first exohedral functionalization of EMFs started from the organosilicon reaction of La@C_{2v}(9)-C_{82} in 1995 [22]. Later on, the digermirane reaction of the La@C_{2v}(9)-C_{82} was also introduced and showed high reactivity [36]. So far, silylation and germylation reactions of mono-EMFs [37], di-EMFs [38,39], and nitride cluster-fullerenes (NCFs) [40,41] have been realized and exhaustively summarized in Kako's and Jin's reviews [35,42].

Very recently, a novel method for the exclusive separation of I_h and D_{5h} isomers of Sc_3N@C_{80} was proposed based on the different reactivity of photoreactions of Sc_3N@I_h-C_{80} and Sc_3N@D_{5h}-C_{80} with disilirane, silirane, and digermirane [43]. Specifically, under the same condition, Sc_3N@I_h-C_{80} reacted readily with them to afford the corresponding 1:1 adducts, whereas Sc_3N@D_{5h}-C_{80} was recovered without any adducts [43]. According to these results, the separation solution was put forward and involved three steps: selective derivatization of Sc_3N@I_h-C_{80} with disilirane, silirane, and digermirane, facile high performance liquid chromatography (HPLC) separation of pristine Sc_3N@I_h-C_{80} and Sc_3N@D_{5h}-C_{80} derivatives, and thermolysis of corresponding derivatives to recovery pristine Sc_3N@I_h-C_{80} [43]. Furthermore, the reaction mechanism has been studied by laser flash photolysis experiments [43]. Decay of the transient absorption of $^3Sc_3N$@I_h-C_{80}* was observed to be enhanced in the presence of disilirane, indicating the quenching process; however, the transient absorption of $^3Sc_3N$@D_{5h}-C_{80}* was much less intensive, which could not confirm the quenching of $^3Sc_3N$@D_{5h}-C_{80}* by disilirane [43]. Finally, based on the time-dependent density functional theory (TD-DFT) calculations, the poor electron acceptor property of $^3Sc_3N$@D_{5h}-C_{80}* might decrease the photochemical reactivity toward disilirane, silirane, and digermirane compared to $^3Sc_3N$@I_h-C_{80}* [43].

2.2. Prato Reaction (1,3 Dipolar Cycloaddition)

The Prato reaction via 1,3-dipolar cycloaddition of azomethine ylides with alkene is one of the most useful methods of fullerene functionalization due to its high selectivity and feasibility [1,2], which means easily connecting a wide range of addends and functional group to fullerenes. Prato reactions of mono-EMFs [44], di-EMFs [27,45], nitride EMFs [28,46], and carbide EMFs [47] have been reviewed in Dunsch's, Yang's, and Jin's reviews [1,2,35]. Herein, recent progress is summarized and some results are inspiring.

The pyrazole and the ring-fused pyrrole reaction of di-EMF $Y_2@C_{3v}(8)$-C_{82} affords highly regioselective and quantitative mono-adduct [48]. Only one [6,6]-adduct out of the twenty-five different types of nonequivalent C-C bonds of $Y_2@C_{3v}(8)$-C_{82} was got and its molecular structure was identified by the single crystal X-ray diffraction [48]. Theoretical results suggested that both the anisotropic distribution of p-electron density on the $C_{3v}(8)$-C_{82} cage and the local strain of the cage carbon atoms lead to the formation of the highly regioselective and quantitative mono-adduct [48]. Additionally, electrochemical studies revealed that the reversibility of the reductive processes of $Y_2@C_{3v}(8)$-C_{82} was significantly changed by exohedral functionalization, whereas the oxidative process was less influenced [48]. The reason for this phenomenon is that the reduction processes depend on the carbon cage, but the oxidation is mainly influenced by the endohedral Y_2 cluster [48].

In 2022, Chen et al. [49] reported the 1,3-dipolar cycloaddition photoreaction of $Sc_3N@D_{3h}$-C_{78} with carbonyl ylide affords two isomeric mono-adducts **1a** and **1b** under light irradiation (see Figure 1a). The single crystal X-ray diffraction confirmed that both mono-adducts **1a** and **1b** have the same addition sites at a closed [6,6] bond and possess the same *cis*-conformation, namely, in which the hydrogen atoms of two methines situated at the same side of the tetrahydrofuran ring with parallel orientation [49]. However, two isomeric mono-adducts **3a** and **3b** were got when $Sc_3N@D_{3h}$-C_{78} was replaced by C_{60} in a similar reaction under the same condition [49]. Surprisingly, the crystal structure of **3b** shows that the addition pattern is located at the closed [6,6]-bond and exhibits a *trans*-conformation, in which the hydrogen atoms of the two methines within the tetrahydrofuran ring located at the opposite sides (see Figure 1b) [49]. In contrast, **3a** has the *cis*-conformation based on the ^{1}H NMR spectrum which has been previously reported by Wang and Yang [50,51]. Furthermore, the DFT calculation results indicated that the synergistic contributions of thermodynamics of adducts, the most reactive C-C bond, and the cis-dipole intermediate from *trans* **2**, result in the high regioselectivity of *cis*-conformations of **1a** and **1b** [49].

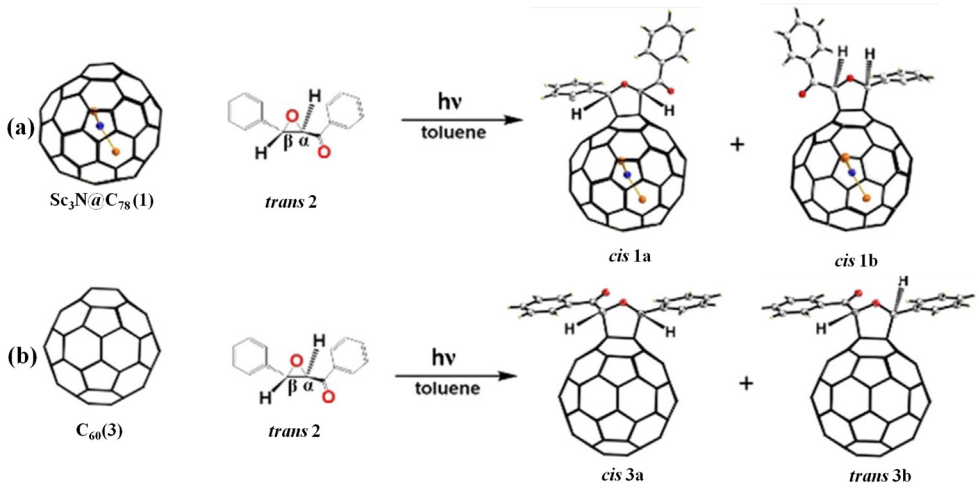

Figure 1. The 1,3-dipolar cycloaddition of *trans*-phenyl-(3-phenyl-oxiranyl)-methanone (*trans* **2**) with (**a**) $Sc_3N@D_{3h}$-C_{78} and (**b**) C_{60}. Atom key: Sc (brown-yellow), N (blue), O (red). Reproduced from Ref. [49] with permission. Copyright 2021 John Wiley and Sons.

Though the mono-adducts of Prato reaction of $M_3N@C_{80}$ (M = M = Sc, Y, Gd, Dy, Ho, Er, Lu) have been widely reported [1,2], the corresponding bis-adducts are rare. Aroua et al. [52] synthesized the bis-adducts of the Prato reaction of $Gd_3N@I_h$-C_{80} and $Y_3N@I_h$-C_{80} in 2015. Later on, Cerón et al. [53] obtained 1,3-dipolar bis-additions of $Sc_3N@I_h$-C_{80} and $Lu_3N@I_h$-C_{80} using the tether-controlled multi-functionalization method, but the unambiguous crystal structure characterization of these reported Prato bis-adducts are missing. Fortunately, Semivrazhskaya et al. [54] reported one precise crystal structure of two bis-ethylpyrrolidinoadducts of $Gd_3N@I_h$-C_{80} (**4**) obtained by regioselective 1,3-dipolar

cycloadditions; see Figure 2a. The crystal structure of the minor-bis-adduct (**7**) shows a C_2-symmetric carbon cage with [6,6][6,6]-addition sites, as shown in Figure 2b and a strictly planar Gd_3N cluster, which is much less strained compared to a pyramidalized cluster of the pristine $Gd_3N@I_h$-C_{80}. Indeed, two interior Gd atoms coordinated to the C_{80} cage at two sp^3 addition sites, releasing the strain of the endohedral Gd_3N cluster in the minor-bis-adduct. However, the structure of major-bis-adduct was presumably asymmetric [6,6][6,6]-addition sites, because its visible - near infrared (vis-NIR) spectra are almost identical to that of the major bis-adduct of $Y_3N@C_{80}$ with an asymmetric [6,6][6,6]-structure. Moreover, it is experimentally observed that the symmetrical minor-bis-adduct of $Gd_3N@I_h$-C_{80} isomerized to the asymmetrical major-adduct and based on the linear transit calculations, a pathway of the isomerization is through the formation of the [6,6][6,6]-bis-adduct, followed by [5,6][6,6]-bis-adduct [54].

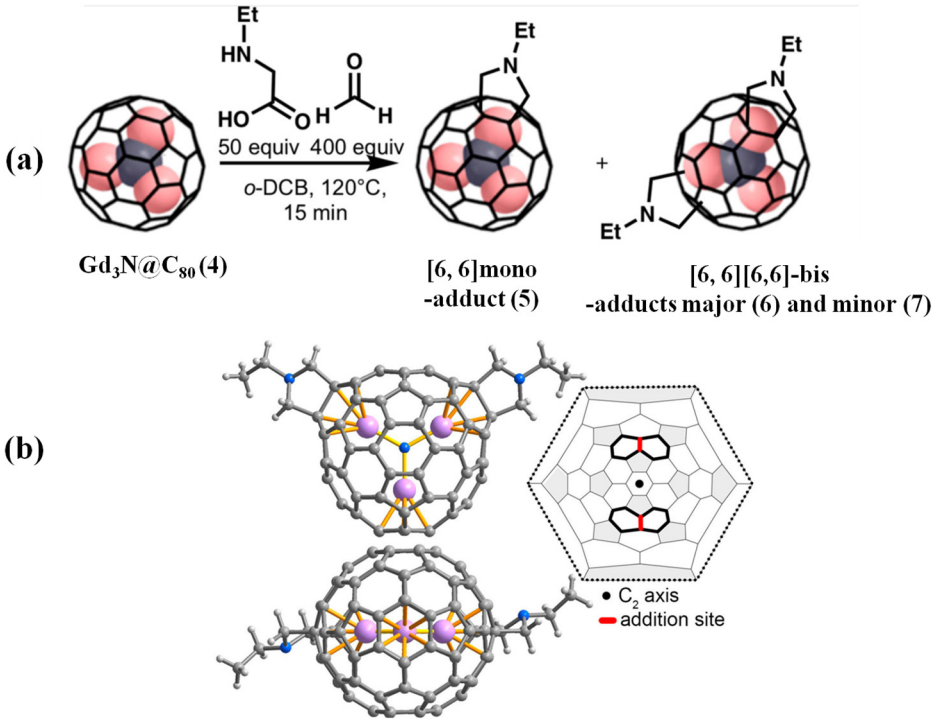

Figure 2. (**a**) Prato reactions of $Gd_3N@I_h$-C_{80} (**4**) afford the mono-adducts (**5**) and bis-adducts (**6**) and (**7**). (**b**) X-ray crystal structure of minor-bis- $Gd_3N@C_{80}[C_4H_9N]_2$ **7** (side and top views) and the red thick bonds in the Schlegel diagram represent the additional sites. The black dot in the center of the Schlegel diagram indicates the C_2 axis. Reproduced from Ref. [54] with permission. Copyright 2019 American Chemical Society.

It is hard to get the Prato multi-additions of EMFs because of their huge isomers theoretically. Unexpectedly, four tris- and one tetra-isomers for both $Y_3N@I_h$-C_{80} and $Gd_3N@I_h$-C_{80} were obtained in a regioselective manner when $M_3N@I_h$-C_{80}(M = Y, Gd) reacted with an excess of N-ethylglycine and formaldehyde [55]. Three of four tris-adducts of $Y_3N@I_h$-C_{80} are [6,6][6,6][6,6] isomers and the remaining one is [6,6][6,6][5,6]-isomer confirmed by the NMR whereas the tetra-adduct is all [6,6] isomer which is similar to that of $Gd_3N@I_h$-C_{80} [55]. And, mutual interconversions among all [6,6] tris-adducts of both $Y_3N@I_h$-C_{80} and $Gd_3N@I_h$-C_{80} are observed at room temperature. Density functional theory (DFT) calculations show that the most stable structures corresponded to adding at the most strained bonds by estimating the relative stabilities of tris- and tetra-adducts formed upon Prato functionalization of the most pyramidalized regions of the fullerene structure [55]. Electron resonance (ESR) measurements of pristine, bis-, and tris-adducts of $Gd_3N@I_h$-C_{80} show that the rotation of the endohedral cluster slowed down as the addition numbers to C_{80} cage increased, which indicates the accommodating of Gd atoms of the relatively large

Gd_3N cluster inner space at the sp^3 addition sites [55]. Therefore, the strain release of the $Gd_3N@I_h$-C_{80} leads to the high regioselectivity of the Prato multi-addition reaction.

2.3. Bingel–Hirsch Reaction

Bingel–Hirsch reaction is one of the most used methods to synthesize derivations of EMFs [1,2]. The first Bingel–Hirsch reaction of $Gd@C_{60}$ affords multi-adducts $Gd@C_{60}[C(COOH)_2]n$ (n = 1–10) [56]. Surprisingly, the reaction of $La@C_{2v}(9)$-C_{82} obtains four singly bonded adducts as well as one conventional cyclopropane adduct [29,57]. Recently, a highly regioselective Bingel–Hirsch reaction of $Y@C_s(6)$-C_{82} induced by the metal encapsulation was reported by Shen et al. [58]. Three mono-adduct out of 44 possible isomers for the $C_s(6)$-C_{82} cage have been thoroughly isolated, showing high regioselectivity [59]. The single-crystal X-ray diffraction crystallography analysis confirmed that the bromomalonate group was singly bonded to the [5,6,6]-cage carbon of $Y@C_s(6)$-C_{82} in one isomer [59]. Meanwhile, further experimental and theoretical results indicate that three mono-adduct isomers may mutually be regioisomers with bromomalonate singly bonded to different cage carbon atoms having high spin density values caused by the encapsulation of a Y^{3+} ion into the low symmetric $C_s(6)$-C_{82} cage [58].

Despite differences in activity, NCFs such as $M_3N@I_h(7)$-C_{80} (M = Sc, Y, Gd, Lu) [59] and $Gd_3N@C_{2n}$ (2n = 82, 84) [60], typically afford the methanofullerene adduct (via [2 + 1] cycloaddition). The Bingel–Hirsch reaction of $Y_3N@I_h(7)$-C_{80} yields an unexpected [6,6]-open mono-adduct confirmed by a crystallographic study [30]. In contrast, the Bingel–Hirsch reaction of $TiY_2N@I_h(7)$-C_{80}, a Y^{3+} ion replaced by a Ti^{3+} ion compared to the $Y_3N@I_h(7)$-C_{80}, affords a singly bonded adduct, indicating that change the endohedral atom or clusters can manipulate the regioselectivity of EMFs as well as the addition pattern [61].

Notably, a new route to synthesize the Bingel–Hirsch derivative of EMFs via the cationic metallofullerenes was reported by Hu et al. recently, as shown in Figure 3 [62]. $M_3N@I_h(7)$-C_{80} (M = Sc or Lu) cations were generated by both electrochemical and chemical oxidation and then the cations successfully underwent the typical Bingel–Hirsch reaction [62]. For $Sc_3N@I_h(7)$-C_{80}, both [5,6]-open (**10**) and [6,6]-open (**11**) adducts have been obtained whereas the former has never been synthesized via the neutral NCFs [62]. However, only a [6,6]-open adduct (**12**) was generated for $Lu_3N@I_h(7)$-C_{80} [62]. DFT calculations implied that the cationic $M_3N@I_h(7)$-C_{80} was much more reactive than the neutral compound for the Bingel–Hirsch reaction [62]. Furthermore, a new unusual mechanism for the Bingel–Hirsch reaction of the cationic NCFs is proposed, involving an outer-sphere single-electron transfer (SET) process [62]. Namely, the diethyl bromomalonate anion not only acts as a nucleophile, the same role in common Bingel–Hirsch reaction, but also as an electron donor, a new role to stable intermediate $[M_3N@C_{80}(C_2H_5COO)_2CBr]^*$ [62]. Additionally, the energy profiles for the Bingel–Hirsch additions on $M_3N@C_{80}^+$ cations for M = Sc and Lu were drawn out to explain the distinguished regioselectivity of $M_3N@C_{80}^+$ cations, in which M = Sc (with the [6,6] and [5,6] products) and M = Lu (with only the [6,6] product) [62].

2.4. Carbene Addition

The carbene reactions are vital for the functionalization of EMFs as well as for determining the molecular structure of EMFs [3]. Up to now, photochemical carbene reactions of mono-EMFs [24], di-EMFs [63], carbide clusterfullerenes [64], and NCFs [65] have been reported and open fulleroid derivatives were usually achieved. Especially, the N-heterocyclic carbene (NHC) reaction of $Sc_3N@I_h$-C_{80} afforded an abnormal carbene product with C5 as its active center singly connected to the inert [6,6,6] carbon atom of the C_{80} cage [66]. In contrast, normal NHC products of $M_3N@I_h$-C_{80} (M = Sc, Lu) were acquired by the introduction of a little oxygen in the same reaction [67]. Recent results of NHC reaction with $Lu_3N@I_h(7)$-C_{80}, $Lu_2@C_{3v}(8)$-C_{82}, and $Lu_2@C_{2v}(9)$-C_{82} indicated that the high regioselectivity and preferential formation for mono-adducts mainly originated from the electronic

effect including molecular orbitals and electrostatic interactions of the fullerene cages in addition to the steric clash between the NHC and EMFs [68].

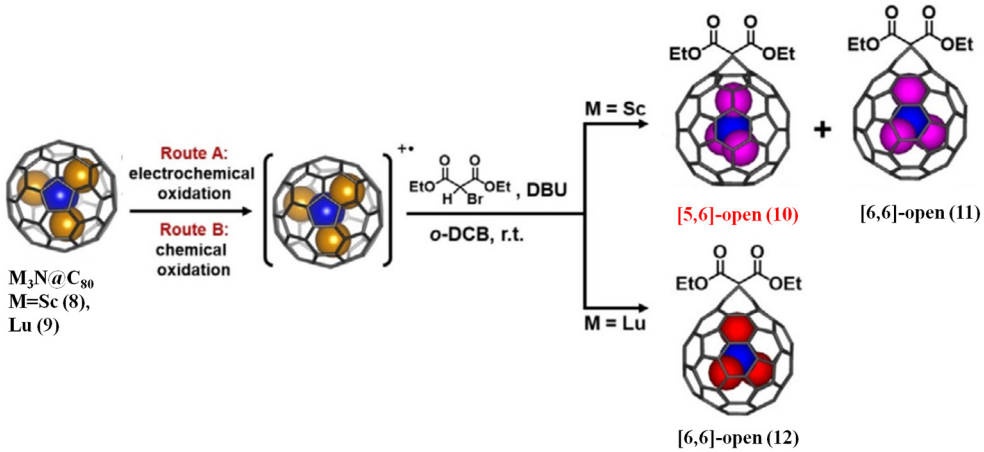

Figure 3. Bingel–Hirsch reaction of $M_3N@I_h$-C_{80} (M = Sc or Lu) radical mono-cation under conventional conditions. Reproduced from Ref. [62] with permission. Copyright 2020 John Wiley and Sons.

Recently, the carbene reaction was extended to the actinide EMFs, Th@C_{3v}(8)-C_{82} and U@C_{2v}(9)-C_{82}, and the former afforded three mono-adducts, named Th@C_{3v}(8)-C_{82}Ad(I, II, III) (Ad = adamantylidene), while four mono-adducts were acquired for the latter, named U@C_{2v}(9)-C_{82}Ad(I, II, III, IV), presenting remarkably higher reactivity than lanthanide EMFs [69], as shown in Figure 4a. Both Th@C_{3v}(8)-C_{82}Ad(I) and U@C_{2v}(9)-C_{82}Ad(I) are [6,6]-open cage structures, which are unambiguously confirmed by single crystal X-ray crystallography [69]. Moreover, isomerization of Th@C_{3v}(8)-C_{82}Ad(II) and Th@C_{3v}(8)-C_{82}Ad(III) and U@C_{2v}(9)-C_{82}Ad(II) and U@C_{2v}(9)-C_{82}Ad(III) was observed at room temperature; however, Th@C_{3v}(8)-C_{82}Ad(I) and U@C_{2v}(9)-C_{82}Ad(I) showed high stability under the same condition [69]. DFT calculations suggested that carbon atoms with the largest negative charge density and POAV(p-orbital axis vector) values are the best sites toward the Ad addition [69]. Furthermore, compared to the lanthanide analogs, the unusually high reactivity of Th@C_{3v}(8)-C_{82} and U@C_{2v}(9)-C_{82} steamed from much closer metal–cage distance, increased metal-to-cage charge transfer, and strong metal–cage interactions, which is due to the significant contribution of extending Th-5f and U-5f orbitals to the occupied molecular orbitals [69].

Very recently, the first carbene reaction of $Dy_2TiC@I_h$-C_{80}, the μ_3-carbido cluster-fullerene (μ_3-CCF) bearing central μ_3-C and Ti(IV) atoms forming a Ti = C double bond, with 2-adamantane-2,3-[3H]-diazirine(AdN_2) was reported [70], see Figure 4b. Noteworthily, the photochemical carbene reaction of $Dy_2TiC@I_h$-C_{80} with AdN_2 affords only one mono-adduct with a [6,6]-open addition pattern, which is unambiguously confirmed by single-crystal X-ray diffraction [70]. Meanwhile, the Ad moiety selectively attacks the [6,6]-bond which is adjacent to the Ti^{4+} ion instead of the two Dy^{3+} ions, thus the encapsulated Ti atom within $Dy_2TiC@I_h$-C_{80}-Ad is fully ordered while the two Dy atoms are still disordered [70]. Theoretical calculations indicate that the [6,6]-open adduct is thermodynamic and the Ti(IV) ion plays a decisive role in the high regioselectivity [70]. In contrast, a different type of adduct with the additional sites adjacent to the Y^{3+} ion instead of the Ti^{3+} ion is predicted to be got when a similar reaction of $Y_2TiN@I_h$-C_{80} containing a Ti(III) ion with AdN_2 is carried out [70]. Hence, the non-rare-earth metal Ti bearing a high oxidation state within the μ_3-CCF determines the peculiarity of the chemical properties of the μ_3-CCF [70].

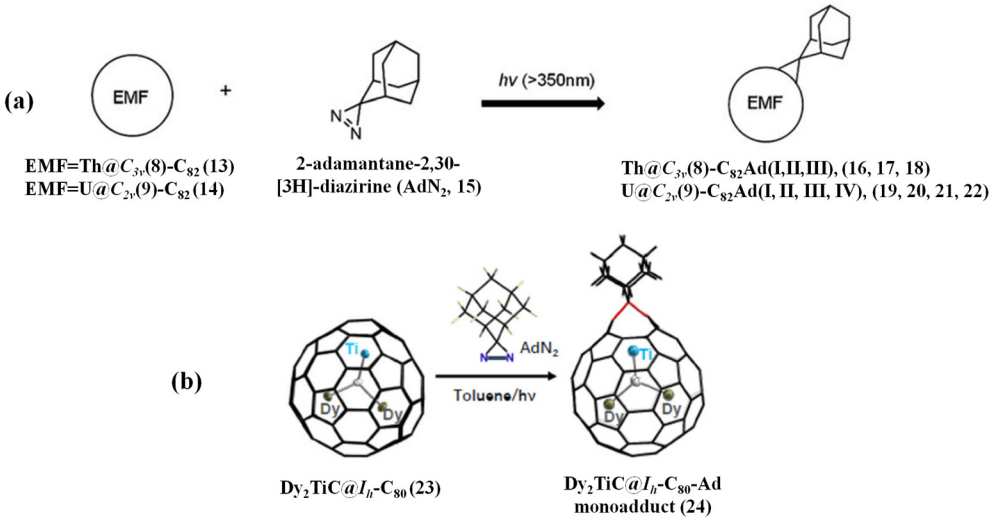

Figure 4. (**a**) Reaction of AdN_2 (AdN_2 = 2-adamantane-2,30-[3H]-diazirine) (**15**) with Th@C_{3v}(8)-C_{82} (**13**) or U@C_{2v}(9)-C_{82} (**14**). Reproduced from Ref. [69] with permission from the Royal Society of Chemistry. (**b**) Synthetic route of $Dy_2TiC@I_h$-C_{80}-Ad (**24**) through the photochemical reaction of $Dy_2TiC@I_h$-C_{80} (**23**) with AdN_2 (**15**). Reproduced from Ref. [70] with permission from the Chinese Chemical Society (CCS), Peking University (PKU), and the Royal Society of Chemistry.

2.5. Radical Addition Reaction

Radical addition reactions of EMFs can generate a wide range of derivatives and especially capture the unstable EMFs to form stable derivatives with a closed-shell electronic configuration. Radical groups such as benzyl or trifluoromethyl were reacted with EMFs including mono-EMFs [71], di-EMFs [31], NFC [72], CCF [32], and cyano-clusters [73] EMFs.

Liu et al. reported that an array of air-stable dimetallofullerene $Ln_2@C_{80}(CH_2Ph)$ (Ln_2 = Y_2, Gd_2, Tb_2, Dy_2, Ho_2, Er_2, TbY, TbGd) (**25**) was acquired by reacting metallofullerene anions with benzyl-bromide in DMF (N,N-Dimethylformamide) solution [74]. Single-crystal X-ray diffraction of $Ln_2@C_{80}(CH_2Ph)$ shows that the benzyl is attached to the cage via a single bond, see Figure 5a [74]. Moreover, there is a covalent lanthanide–lanthanide bond in $Ln_2@C_{80}(CH_2Ph)$ and a single electron residing on the metal–metal bonding orbital [74]. Thanks to very strong exchange interactions between 4f moments and the residing single electron, $Tb_2@C_{80}(CH_2Ph)$ is a robust nanomagnet and shows a gigantic coercivity of 8.2 Tesla at 5 K and a high 100 s blocking temperature of magnetization of 25.2 K [74].

Recently, a long-sought dysprosium-based EMF Dy@C_{2v}(5)-C_{80} was captured in the form of Dy@C_{2v}(5)-$C_{80}(CH_2Ph)$(Ph =-C_6H_5) (**26**) from carbon soot with various fullerenes [75]. On the basis of the single crystal X-ray diffraction, the carbon cage is confirmed as a rare C_{2v}(5)-C_{80}, which is the first case of an EMF composed of a mono-metal rare earth ion encapsulated within this C_{80} cage, as shown in Figure 5b [75]. And, the benzyl group is grafted onto the [5,6,6]-carbon atom via a single bond, which verifies that Dy@C_{2v}(5)-$C_{80}(CH_2Ph)$ has an open-shell electron configuration and its electron configuration is $Dy^{3+}@C_{2v}(5)\text{-}C_{80}^{3-}$ [75]. Meanwhile, the encapsulated Dy^{3+} ion is sited underneath the [6,6]-bond and deviated from the symmetry plan of C_{2v}(5)-C_{80} [75]. Furthermore, based on theoretical calculations, the bandgap is enlarged from 1.11 eV to 1.86 eV and the LUMO energy level is obviously elevated to about 0.87 eV due to a benzyl radical addition to Dy@C_{2v}(5)-C_{80}, thus synergistically stabilizing the missing Dy@C_{2v}(5)-C_{80} [75].

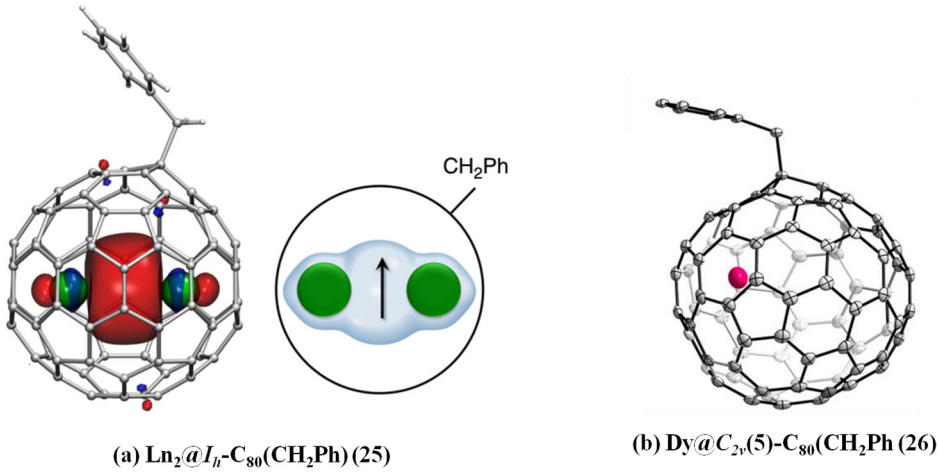

Figure 5. (**a**) Molecular structure of $Ln_2@C_{80}(CH_2Ph)$. Single-occupied Ln–Ln bonding molecular orbital (left; carbons are gray, hydrogens are white, lanthanides are green), and schematic depiction of the molecule (right; the arrow represents an unpaired electron residing on the Ln–Ln bonding orbital). (**b**) Drawing of $Dy@C_{2v}(5)$-$C_{80}(CH_2Ph)$.

Xu et al. reported that using 1,2,4-trichlorobenzene or iodobenzene to extract the Er-based fullerene soot, $Er@C_{72}(C_6H_3Cl_2)$ and $Er@C_{76}(C_6H_5)$ were obtained by free radical addition [76]. In addition, a high-temperature trifluoromethylated reaction of $Er@C_{2n}$ and $AgCOOCF_3$ afforded several adducts, $Er@C_{76}(CF_3)_5$, $Er@C_{82}(CF_3)_3$, and $Er@C_{82}(CF_3)_5$(I, II, III) [76]. Unexpectedly, all derivatives of $Er@C_{2n}$(2n = 72, 76, 82) exhibit detectable characteristic NIR photoluminescence at around 1520 nm, which stems from the emission of Er^{3+}, but pristine $Er@C_{2n}$(2n = 76, 82) show no photoluminescence [76]. Based on the UV-vis-NIR absorption spectrum, HOMO-LUMO gaps of the derivatives are remarkably enlarged compared to that of pristine $Er@C_{2n}$ [76]. And, odd-number addition groups result in a closed-shell electronic structure for the derivatives [76]. Hence, the enlarged HOMO-LUMO gap and the closed-shell electronic structure turn on the photoluminescence activity of Er^{3+} [76]. In addition, the photoluminescence mechanism study suggests that the photoluminescence of the Er^{3+} ion comes from the energy transfer from the fullerene cage to the Er^{3+} ion; however, the photoluminescence of pristine $Er@C_{2n}$ was quenched by energy transfer from the first excited state of Er^{3+} to the fullerene cage [76].

Li et al. reported a novel radical reaction of $Y@C_{2v}(9)$-C_{82} with N-arylbezamidine catalyzed by silver carbonate [77]. The reaction is highly regioselective and affords only one mono-adduct with an imidazoline group. The theoretical calculation reveals the addition group is attached to a specific [5,6]-bond near the Y atom [77].

2.6. Electrophilic Trifluoromethylation

The lack of selectivity of the radical addition reactions results in multi-adducts and a complicated separation process. Unprecedentedly, the high selectivity of electrophilic trifluoromethylation of metallofullerene anions was reported very recently [78]. Specifically, reacting metallofullerene anions extracted by DMF with Umemoto reagent II affords $M_2@C_{80}(CF_3)$ (M = Tb, Y) mono-adducts as the major product, indicating higher selectivity of electrophilic trifluoromethylation than that of benzyl bromide reaction (see Figure 6a) [78]. The single-crystal X-ray diffraction analysis shows that the CF_3 group is attached to the pentagon/hexagon/hexagon junction ([5,6,6] position) of the I_h-C_{80} cage via a single bond, as shown in Figure 6b [78]. Similarly, a single electron remains between two Tb ions, forming single-electron metal–metal bonds with the formal metal oxidation state of $Tb^{2.5+}$ [78]. As expected, $Tb_2@C_{80}(CF_3)$ is also a robust single-molecule magnet based on magnetic characterizations, which is comparable to the benzyl mono-adduct $Tb_2@C_{80}(CH_2Ph)$ [78]. Therefore, electrophilic trifluoromethylation is a very excellent approach to stabilize metallofullerene anions $M_2@C_{80}$, which is a simple, fast room-temperature reaction with high

selectivity and needs less time for required HPLC separation compared to the benzylation reaction of $M_2@C_{80}$ [78].

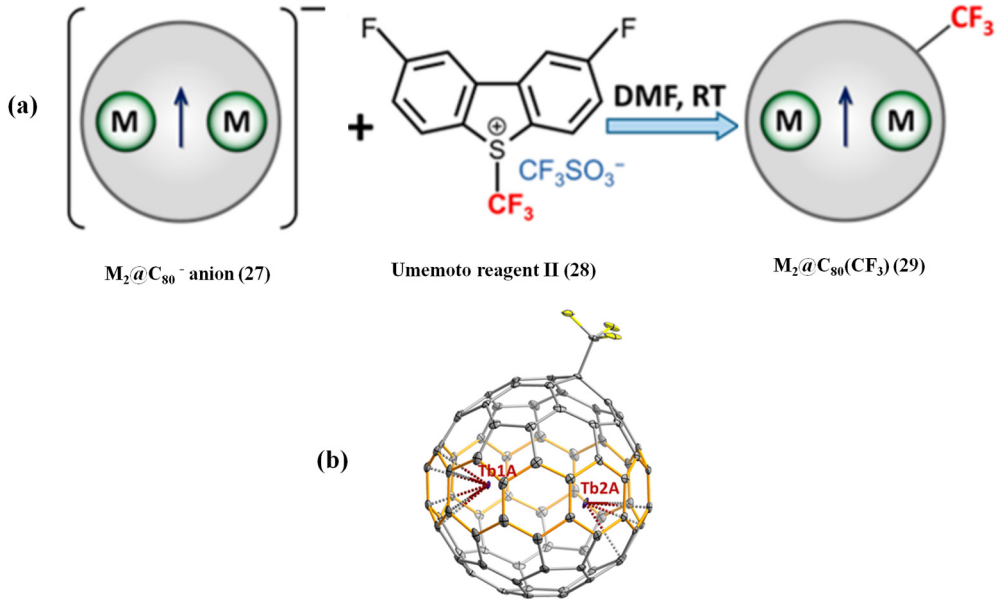

Figure 6. (**a**) Scheme of the reaction between $M_2@C_{80}^-$ anion and Umemoto reagent II with the formation of $M_2@C_{80}(CF_3)$. (**b**) $Tb_2@C_{80}(CF_3)$ molecule from the single crystal showing the main Tb sites Tb1A and Tb2A. Reproduced from Ref. [78] with permission. Copyright 2021 American Chemical Society.

2.7. Coordination Reaction

The organometallic complexes of EMFs usually bear the η^2 coordination fashion [79], and the η^1-coordinated complexes of EMFs with only one metal–cage bond are very desirable. Until 2019, Xie et al. [80] reported a coordination reaction of $Re_2(CO)_{10}$ (**31**) to paramagnetic $Y@C_{2v}(9)$-C_{82} (**30**) by an efficient radical coupling, and an unprecedented η1-coordinated complex: $Re(CO)_5$-η^1-$Y@C_{2v}(9)$-C_{82} (**32**) was obtained, as shown in Figure 7a. Crystallographic results confirmed that the $Re(CO)_5$ moiety coordinates to a [5,6,6]-carbon atom of the C_{82} cage via a single Re-C σ bond [80]. Furthermore, Vis-NIR and ESR results verified that the $Re(CO)_5$ moiety transfers one electron to the EMF, resulting in a closed-shell electronic structure similar to anionic ($Y@C_{82}$)- species with high stability [80]. In contrast, replacing with diamagnetic $Sc_3N@I_h(9)$-C_{82} and $Lu_2@C_{2v}(9)$-C_{82} in the same reaction, no product is yielded, further confirming a radical coupling process [80].

Bao et al. [81] reported that reacting mono-metallofullerenes, $Eu@C_2(5)$-C_{82} (**33**) and $Eu@C_2(13)$-C_{84}) (**34**), with a tungsten complex $W(CO)_4(Ph_2PC_2H_4PPh_2)$ (**35**) afford the highly regioselective product; alternatively, only one product was acquired for each reaction. Single crystal X-ray crystallography shows that in both products (**36**, **37**), the tungsten moiety coordinates to a [6,6]-bond of the cage with an η^2-fashion, as shown in Figure 7b [81]. And, after the coordination of the tungsten moiety, the motion of the internal Eu ion in both adducts is restricted to a certain extent, which is due to changing the electrostatic potentials inside the cage supported by theoretical calculations [81]. Moreover, the observed high regioselectivity is explained by electron transfer from the endohedral Eu to the cage, which significantly changed the LUMO distribution on $C_2(5)$-C_{82}/$C_2(13)$-C_{84} based on theoretical calculations [81]. Therefore, the interplay between the endohedral and the exohedral metallic moiety is achieved in a single molecule system via intramolecular charge transfer [81].

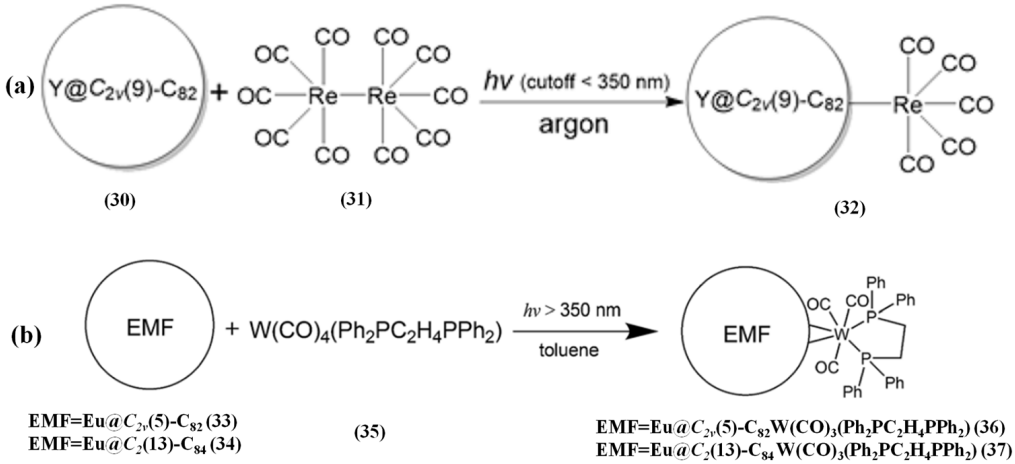

Figure 7. (**a**) Reaction scheme of Y@C_{2v}(9)-C_{82} with $Re_2(CO)_{10}$. Reproduced from Ref. [80] with permission from the Royal Society of Chemistry. (**b**) Reaction of $W(CO)_4(Ph_2PC_2H_4PPh_2)$ with Eu@C_2(5)-C_{82} or Eu@C_2(13)-C_{84}. Reproduced from Ref. [81] with permission. Copyright 2019 American Chemical Society.

2.8. Methoxide Reaction

Unexpected bis-methoxyl adducts of Sc_3N@I_h-C_{80} were got for the first time when Sc_3N@I_h-C_{80} reacted with/without $Ph_2C{=}O$, PhC≡CPh or PhC≡N in the presence of tetrabutylammonium hydroxide (TBAOH) stored in CH_3OH [82]. However, it was further observed that bis-methoxyl adducts of Sc_3N@I_h-C_{80} form irrespective of the presence of other reagents, since TBAOH in CH_3OH efficiently boosts the -CH_3O addition [82]. Furthermore, single crystal X-ray diffraction analysis unambiguously determines the molecular structures of the products as 1,4- and 1,2-bis-methoxyl adducts, and the conformations of the two -OCH_3 groups in both bis-methoxyl adducts are obviously different bis-methoxyl, as shown in Figure 8a,b [82]. And, the planar Sc_3N cluster in 1,4-bis-methoxyl adducts (**38**) is orthogonal with the plane crossing the addition sites, whereas the metal cluster in 1,2-bis-methoxyl adducts (**39**) is nearly parallel to the plane crossing the addition site, which indicates that exohedral modification is practical to control the orientation of the embedded cluster bis-methoxyl [82]. In addition, a possible mechanism related to an anion addition and a radical reaction was put forward (see Figure 8c), which opened up new horizons to the highly selective reactions between the methoxyl anion and EMFs [82]. Specifically, CH_3O- generated by deprotonates CH_3OH via TBAOH prevailed over OH- (from TBAOH) in the o-DCB (o-dichlorobenzene) solution and attached to Sc_3N@C_{80} to form the mono-anion $[Sc_3N@C_{80}(OCH_3)]^-$ firstly [82]. Then, the mono-anion was oxidized to $[Sc_3N@C_{80}(OCH)$•radical by I_2, and the dimethoxyfullerene anion $[Sc_3N@C_{80}(OCH_3)_2]^-$ formed by accepting another CH_3O^- [82]. Finally, the ultimate 1,2- or 1,4-addition dimethoxyfullerene products were yielded through the oxidation of dimethoxyfullerene anion by I_2 [82].

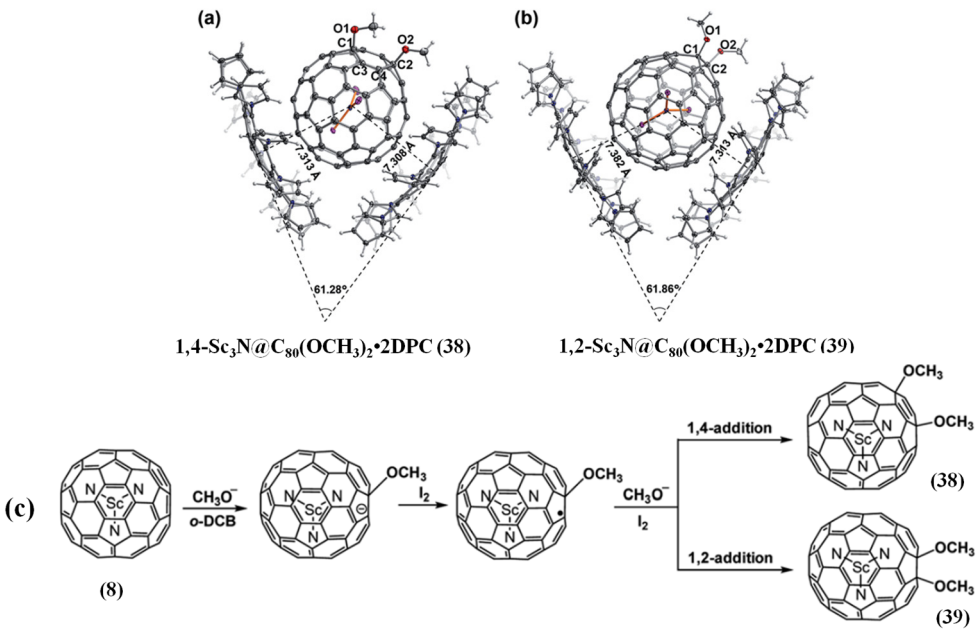

Figure 8. Single crystal X-ray structures of co-crystals 1,4-$Sc_3N@C_{80}(OCH_3)_2$•2DPC (**a**) and (**b**) 1,4-$Sc_3N@C_{80}(OCH_3)_2$•2DPC with thermal ellipsoids at the 10% probability level. (**c**) Plausible mechanism of the reaction between $Sc_3N@I_h$-C_{80} and TBAOH/CH_3OH in o-DCB. Reproduced from Ref. [82] with permission from the Royal Society of Chemistry.

2.9. Multicomponent Reactions

Very recently, pyrazoline-fused metallofullerene derivative (**41**) as shown in Figure 9 was generated from a four-component cascade reaction of $Sc_3N@I_h$-C_{80} with 3,6-di(pyridin-2-yl)-1,2,4,5-tetrazines (**40**), H_2O, and O_2 [83]. The [5,6] pyrazoline-fused structure is remarkably different from the reaction of a 1,2,4,5-tetrazine with $Sc_3C_2@I_h$-C_{80} which provided a bis-fulleroid derivative [84]. Moreover, the reaction was extended to 3,6-bis(6-methylpyridin-2-yl)-1,2,4,5-tetrazine, and a similar [5,6] pyrazoline-fused derivative (**42**) was achieved [83]. Furthermore, a plausible formation mechanism of pyrazoline-fused metallofullerenes is proposed, which involved a complicated sequence of Diels–Alder reaction, retro Diels–Alder reaction with N_2 extrusion, hydration reaction, rearrangement reaction, and oxidative dehydrogenation reaction [83].

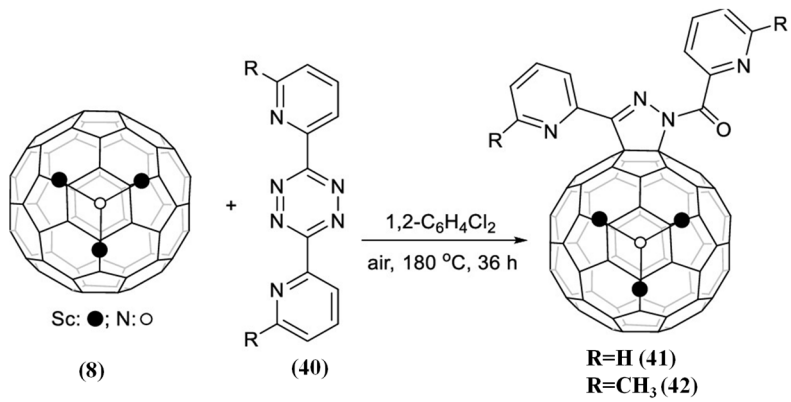

Figure 9. The reaction of $Sc_3N@I_h$-C_{80} with tetrazines (**40**). Reproduced from Ref. [83] with permission. Copyright 2022 American Chemical Society.

Table 1. An exhaustive list of functionalizations of EMFs reported from 2019 to date.

Reaction	Endohedral Metallofullerene	Reactants	Product	Addition Position	Number of Isomers	Ref.
Silylation and germylation	$Sc_3N@I_h$-C_{80}	Disilirane	$Sc_3N@C_{80}Si_2Mes_4$	[1,2], [1,4]	2	[40,43]
		Silirane	$Sc_3N@C_{80}Si(Dep)_2CH_2CHtBp$	[5,6]diastereomers,[6,6]	3	[43]
		Digermirane	$Sc_3N@C_{80}Ge(Dep)_4$	[1,4]	1	[43]
	$Sc_3N@D_{5h}$-C_{80}	Disilirane, silirane, digermirane	No product	non-reactive	0	[43]
Prato reaction (1,3 dipolar cycloaddition)	$Y_2@C_{3v}(8)$-C_{82}	Diphenylnitrilimine ylide	$Y_2@C_{82}N_2(C_6H_5)_2$	[6,6]	1	[48]
		N-benzylazomethine ylide	$Y_2@C_{82}NCH_2(C_6H_5)$	[6,6]	1	[48]
	$Sc_3N@D_{3h}$-C_{78}	Trans-phenyl-(3-phenyl-oxiranyl)-methanone	$Sc_3N@C_{78}(C_6H_5)CHOCHCO(C_6H_5)$	cis-[6,6]	2	[49]
	$Gd_3N@I_h$-C_{80}	N-ethylglycine, paraformaldehyde	$Gd_3N@C_{80}((CH_2)_2NEt)_2$	[6,6] [6,6]-bis adduct	2	[54]
			$Gd_3N@C_{80}((CH_2)_2NEt)_3$	[6,6] [6,6] [6,6] tris-adduct	3	[55]
			$Gd_3N@C_{80}((CH_2)_2NEt)_3$	[6,6] [6,6] [5,6] tris-adduct	1	[55]
			$Gd_3N@C_{80}((CH_2)_2NEt)_4$	all [6,6] tera-adduct	1	[55]
Bingel–Hirsch reaction	$Y@C_s(6)$-C_{82}	Diethyl bromomalonate, DBU	$Y@C_{82}CBr(CCOOCH_2CH_3)_2$	[5,6,6]-single bond	3	[58]
	$Sc_3N@I_h(7)$-C_{80}	Diethyl bromomalonate, DBU	$Sc_3N@C_{80}$ $CBr(CCOOCH_2CH_3)_2$	[5,6]-open, [6,6]-open	2	[62]
	$Lu_3N@I_h(7)$-C_{80}	Diethyl bromomalonate, DBU	$Lu_3N@C_{80}$ $CBr(CCOOCH_2CH_3)_2$	[6,6]-open	1	[62]
Carbene addition	$Th@C_{3v}(8)$-C_{82}	2-adamantane-2,30-[3H]-diazirine(AdN_2)	$Th@C_{82}Ad$	[6,6]-open, et al.	3	[69]
	$U@C_{2v}(9)$-C_{82}	2-adamantane-2,30-[3H]-diazirine(AdN_2)	$U@C_{82}Ad$	[6,6]-open, et al.	4	[69]
	$Dy_2TiC@I_h$-C_{80}	2-adamantane-2,3-[3H]-diazirine (AdN_2)	$Dy_2TiC@C_{80}$-Ad	[6,6]-open	1	[70]

Table 1. *Cont.*

Reaction	Endohedral Metallofullerene	Reactants	Product	Addition Position	Number of Isomers	Ref.
Radical addition reaction	$Ln_2@C_{80}$(Ln_2 = Y_2, Gd_2, Tb_2, Dy_2, Ho_2, Er_2, TbY, TbGd)	$BrCH_2Ph$	Ln2@C80(CH2Ph)	[5,6,6]	1	[74]
	$Dy@C_{2v}(5)$-C_{80}	$BrCH_2Ph$	Dy@C80(CH2Ph)	[5,6,6]	1	[75]
	$Er@C_{72}$	1,2,4-trichlorobenzene	$Er@C_{72}(C_6H_3Cl_2)$	Unknown	1	[76]
	$Er@C_{76}$	Iodobenzene	$Er@C_{76}(C_6H_5)$	Unknown	1	[76]
		$AgCOOCF_3$	Er@C76(CF3)5	Unknown	1	[76]
	$Er@C_{82}$	$AgCOOCF_3$	Er@C82(CF3)3	Unknown	1	[76]
			Er@C82(CF3)5	Unknown	3	[76]
	$Y@C_{2v}(9)$-C_{82}	N-arylbezamidine	$Y@C_{82}NPhCNPh$	[5,6]	1	[77]
Electrophilic trifluoromethylation	$Tb_2@C_{80}^-$	Umemoto reagent II	$Tb_2@C_{80}(CF_3)$	[5,6,6]	1	[78]
	$Y_2@C_{80}^-$	Umemoto reagent II	$Tb_2@C_{80}(CF_3)$	[5,6,6]	1	[78]
Coordination reaction	$Y@C_{2v}(9)$-C_{82}	$Re_2(CO)_{10}$	$Re(CO)_5$-η^1-$Y@C_{2v}(9)$-C_{82}	[5,6,6]	1	[80]
	$Eu@C_2(5)$-C_{82}	$W(CO)_4(Ph_2PC_2H_4PPh_2)$	$Eu@C_{82}$ $W(CO)_3(Ph_2PC_2H_4PPh_2)$	η^2-[6,6]-bond	1	[81]
	$Eu@C_2(13)$-C_{84}	$W(CO)_4(Ph_2PC_2H_4PPh_2)$	$Eu@C_{84}$) $W(CO)_3(Ph_2PC_2H_4PPh_2)$	η^2-[6,6]-bond	1	[81]
Methoxide reaction	$Sc_3N@I_h$-C_{80}	TBAOH, CH_3OH	$Sc_3N@C_{80}(OCH_3)_2$	[1,2], [1,4]	2	[82]

Table 1. *Cont.*

Reaction	Endohedral Metallofullerene	Reactants	Product	Addition Position	Number of Isomers	Ref.
Multicomponent reactions	$Sc_3N@I_h$-C_{80}	3,6-di(pyridin-2-yl)-1,2,4,5-tetrazines, water, and oxygen	$Sc_3N@C_{80}CN{=}NCO(C_5NH_4)_2$	[5,6]-closed	1	[83]
		3,6-bis(6-methylpyridin-2-yl)-1,2,4,5-tetrazine, water, and oxygen	$Sc_3N@C_{80}CN{=}NCO(C_5NCH_3)_2$	[5,6]-closed	1	[83]
	$Lu_3N@I_h$-C_{80}	tBuNC and EWG-bearing terminalalkynes	$Lu_3N@C_{80}CCR^1CONHtBuCOR^2$	[6,6]-open	1	[85]
		tBuNC and dimethyl acetylenedicarboxylate (DMAD)	$Lu_3N@C_{80}C(COOMe)C(COOMe)CNtBu$	[6,6]-open	1	[85]
Difluoromethylenation reaction	$Sc_3N@I_h$-C_{80}	$CF_2ClCOONa$	$Sc_3N@C_{80}(CF_2)$	[6,6]-open	1	[86]
	$Sc_3N@C_{78}$	$CF_2ClCOONa$	$Sc_3N@C_{78}(CF_2)$	[6,6]	1	[87]

Unexpected formation of metallofulleroids with [6,6]-open structure from the isocyanide-based multicomponent reactions of an isocyanide (e.g., tBuNC), various alkynes, and $Lu_3N@I_h$-C_{80} have been reported recently [85]. A major product was obtained by using EWG (electron-withdrawing group)-bearing terminal alkynes, whereas no products were obtained by using disubstituted internal alkynes [85]; see Figure 10a. Notably, when $Lu_3N@Ih$-C_{80} was replaced by C_{60}, there were no isolated products under any conditions [85]. Surprisingly, unlike internal alkynes, dimethyl acetylenedicarboxylate (DMAD) yielded a ketenimine metallofulleroid **45**, as shown in Figure 10b, while the addition pattern is greatly different from that of C_{60} reacting with the same reactants [85]. Strikingly, a variable temperature single-crystal study of metallofulleroid **46** showed that the motion of the embedded cluster is significantly hindered by the close interaction with the exohedral organic appendant of a neighboring molecule [85]. Furthermore, DFT calculations suggested that the reaction mechanism involved three main steps including a barrierless anionic attack of the dipole, 3-exo-trig ring closure, and final hydration [85].

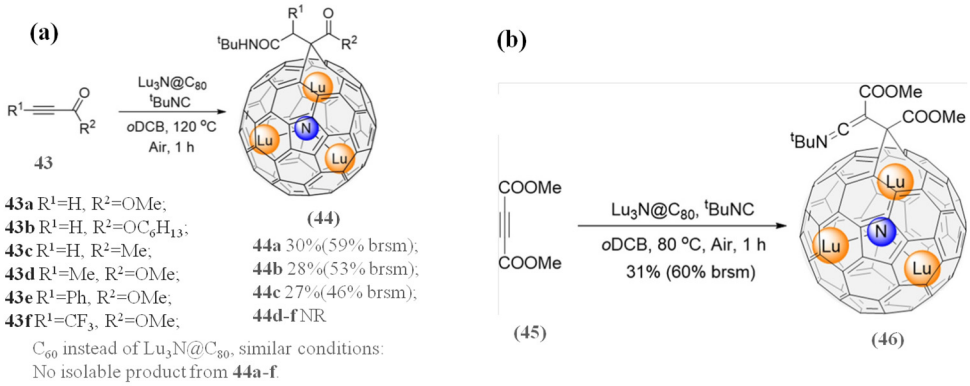

Figure 10. (**a**) Preparation of **44a**−**c** reacted from alkyl isocyanides and alkynes. Brsm = based on recovered starting material; NR = No reaction. (**b**) Synthesis of a ketenimine metallofulleroid **46**. Reproduced from Ref. [85] with permission. Copyright 2021 John Wiley and Sons.

2.10. Difluoromethylenation Reaction

Recently, difluoromethylenation of $Sc_3N@I_h$-C_{80} reacting with $CF_2ClCOONa$ affords a sole C_s-symmetric $Sc_3N@C_{80}(CF_2)$ adduct [86]. Based on the ^{19}F, ^{13}C, and ^{45}Sc NMR spectroscopic, $Sc_3N@C_{80}(CF_2)$ was identified as the [6,6]-open structure with 2.2–2.3 Å between the bridgehead atoms, which is consistent with the DFT-optimized structure (see Figure 11) [86]. And the UV/vis spectra of $Sc_3N@C_{80}(CF_2)$ are similar to that of $Sc_3N@I_h$-C_{80}, thus indicating the [6,6]-open structure with weakly perturbed π-electron systems [86]. Furthermore, the electrochemical behavior of $Sc_3N@C_{80}(CF_2)$ resembles that of $Sc_3N@I_h$-C_{80}, in which both the HOMO and LUMO level of $Sc_3N@C_{80}(CF_2)$ downshift 0.1 eV compared to the pristine $Sc_3N@I_h$-C_{80}, resulting in essentially unchanged HOMO–LUMO gap [86]. It is worth noting that in the experiment the absence of the [5,6]-conformer, the more energetically favorable one based on the theoretical analysis, suggests that the adduct is kinetical rather than thermodynamical [86]. In addition, the nucleophilic route, which involves nucleophilic addition of CF_2Cl^- anion followed by cyclopropanation via Cl^- displacement, is considered to be better than the route of [2 + 1]-cycloaddition of CF_2 carbene [86].

Very recently, the difluoromethylenation reaction was extended to $Sc_3N@C_{78}$ and it showed higher reactivity than $Sc_3N@C_{80}$, in which the reaction temperature is lower [87]. Mono-adduct $Sc_3N@C_{78}(CF_2)$ was identified by the mass spectrum, but, unfortunately, the $Sc_3N@C_{78}(CF_2)$ degraded rapidly, which was different from $Sc_3N@C_{80}(CF_2)$ and the CF_2 adducts of empty fullerenes [87]. And, only the UV-Vis spectrum of the $Sc_3N@C_{78}(CF_2)$ was recorded and showed high similarity with the spectra of the Bingel–Hirsch mono-adduct and that of the major Prato mono-adduct, indicating that $Sc_3N@C_{78}(CF_2)$ has the same bond type, bond 66-6 [87]. Moreover, DFT results suggested that the open [6,6]-$Sc_3N@C_{78}(CF_2)$

is more stable and the regioselectivity is controlled kinetically as well as the CF_2 addition mechanism resembles that of $Sc_3N@C_{80}$ [87].

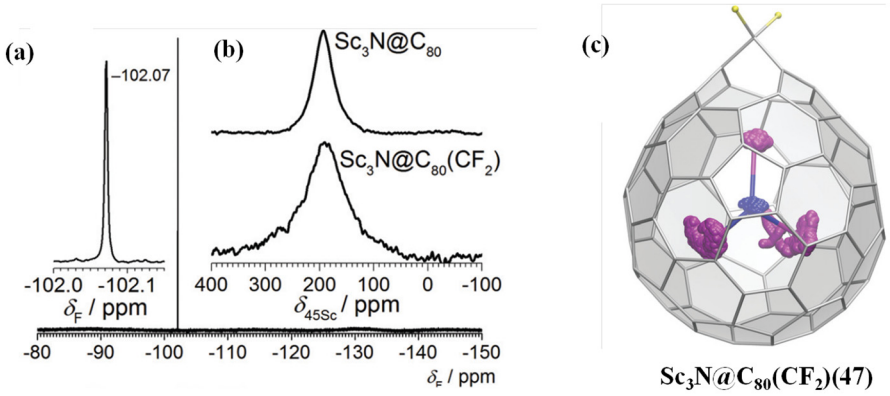

Figure 11. (**a**) ^{19}F NMR spectra of $Sc_3N@C_{80}(CF_2)$. (**b**) Room temperature ^{45}Sc NMR spectra of $Sc_3N@I_h-C_{80}$ (top) and $Sc_3N@C_{80}(CF_2)$ (bottom). (**c**) DFT molecular dynamics trajectories for $Sc_3N@C_{80}(CF_2)$ (100 ps), C atoms are magenta, and N is blue. Reproduced from Ref. [86] with permission from the Royal Society of Chemistry.

3. Conclusions and Outlook

In summary, EMFs exhibit active reactivities toward versatile functionalization reactions, which confer EMFs tunable properties. Prato reaction was extended to EMFs with low symmetry, such as $Sc_3N@C_{78}$ and $Y_2@C_{3v}(8)$-C_{82}; furthermore, the complicated bis-adducts and multi-adducts of Prato reaction were studied as well. Metal encapsulation induces a highly regioselective Bingel–Hirsch adducts of $Y@C_s(6)$-C_{82} achieved and a new cationic metallofullerene route was put forward for Bingel–Hirsch reaction. Carbene additions of actinide EMFs and Ti-based EMFs were developed. A new non-cycloaddition of EMFs, methoxide reaction, was exploited. Furthermore, new complicated multi-component reactions instead of simple transplantation from empty fullerenes arise and acquire unexpected adducts, expanding new horizons in the functionalization of EMFs. Especially, besides radical reactions, new electrophilic trifluoromethylation was exploited to stabilize the missing EMFs.

High regioselectivity is frequently observed for EMFs due to strong metal–cage interactions. The endohedral cluster plays an important role in determining the regioselectivity and addition pattern. Furthermore, combined with calculated results, the regioselectivity of the reactions was plausibly interpreted by POAV, HOMOs/LUMOs, and charges. However, new credible, advanced, and reasonable theoretical calculation schemes are also expected. In turn, the addition groups affect the location, motion, orientation, and electronic state of the encapsulated clusters. As a result, the ultimate structures and properties of the derivatives of EMFs are together regulated by the intramolecular interplay of the cluster, carbon cage, and exohedral groups.

Recent functionalization reactions are mainly restricted to exploring the inherent chemical activities of EMFs or stabilizing EMFs. However, using reaction groups to modulate the magnetic, luminescence, or photovoltaic properties of EMFs is rarely reported. And it is not much clear whether and how the type or amount of reaction groups affects those properties of EMFs. Therefore, more efforts are needed to reveal the relationships between the reaction groups and those properties of EMFs and make metallofullerenes truly applicable materials. Functionalizations of EMFs are an attractive and popular area of fullerene research, which still holds great promise.

Author Contributions: Conceptualization, S.W.; Methodology, X.T., H.L., S.D. and S.W.; Writing—Original Draft, S.W.; Visualization, B.Y., X.L. and Y.H.; Writing—Review and Editing, X.Z., S.W. and F.J. All authors have read and agreed to the published version of the manuscript.

Funding: This work is supported by the National Natural Science Foundation of China (No. 22201028, No. 52002365); the China Postdoctoral Science Foundation (No. 2022M720587); the Postdoctoral Special Funding Program of the Chongqing Human Resources and Social Security Bureau (No. 2021XM1017); the Science and Technology Research Program of Chongqing Municipal Education Commission (NO. KJQN202100823); and the Natural Science Foundation of Chongqing Technology and Business University (2152014).

Data Availability Statement: No new data were created.

Conflicts of Interest: The authors declare no conflict of interest.

References

1. Popov, A.A.; Yang, S.F.; Dunsch, L. Endohedral Fullerenes. *Chem. Rev.* **2013**, *113*, 5989–6113. [CrossRef] [PubMed]
2. Yang, S.F.; Wei, T.; Jin, F. When metal clusters meet carbon cages: Endohedral clusterfullerenes. *Chem. Soc. Rev.* **2017**, *46*, 5005–5058. [CrossRef] [PubMed]
3. Lu, X.; Feng, L.; Akasaka, T.; Nagase, S. Current status and future developments of endohedral metallofullerenes. *Chem. Soc. Rev.* **2012**, *41*, 7723–7760. [CrossRef] [PubMed]
4. Cai, W.T.; Chen, C.H.; Chen, N.; Echegoyen, L. Fullerenes as nanocontainers that stabilize unique actinide species inside: Structures, formation, and reactivity. *Acc. Chem. Res.* **2019**, *52*, 1824–1833. [CrossRef] [PubMed]
5. Meng, Q.Y.; Abella, L.; Yao, Y.R.; Sergentu, D.; Yang, W.; Liu, X.Y.; Zhuang, J.X.; Echegoyen, L.; Autschbach, J.; Chen, N. A charged diatomic triple-bonded U≡N species trapped in C_{82} fullerene cages. *Nat. Commun.* **2022**, *13*, 7192. [CrossRef] [PubMed]
6. Zhuang, J.X.; Morales-Martínez, R.; Zhang, J.W.; Wang, Y.F.; Yao, Y.R.; Pei, C.Y.; Rodríguez-Fortea, A.; Wang, S.A.; Echegoyen, L.; Graaf, C.D.; et al. Characterization of a strong covalent Th^{3+}-Th^{3+} bond inside an I_h(7)-C_{80} fullerene cage. *Nat. Commun.* **2021**, *12*, 2372. [CrossRef] [PubMed]
7. Shinohara, H. Endohedral metallofullerenes. *Rep. Prog. Phys.* **2000**, *63*, 843–892. [CrossRef]
8. Xu, W.; Feng, L.; Calvaresi, M.; Liu, J.; Liu, Y.; Niu, B.; Shi, Z.J.; Lian, Y.F.; Zerbetto, F. An experimentally observed trimetallofullerene $Sm_3@I_h$-C_0. *J. Am. Chem. Soc.* **2013**, *135*, 4187–4190. [CrossRef]
9. Stevenson, S.; Rice, G.; Glass, T.; Harich, K.; Cromer, F.; Jordan, M.R.; Craft, J.; Hadju, E.; Bible, R.; Olmstead, M.M.; et al. Small-bandgap endohedral metallofullerenes in high yield and purity. *Nature* **1999**, *401*, 55–57. [CrossRef]
10. Wang, C.R.; Kai, T.; Tomiyama, T.; Yoshida, T.; Kobayashi, Y.; Nishibori, E.; Takata, M.; Sakata, M.; Shinohara, H. A scandium carbide endohedral metallofullerene: $(Sc_2C_2)@C_{84}$. *Angew. Chem. Int. Ed.* **2001**, *40*, 397–399. [CrossRef]
11. Svitova, A.L.; Ghiassi, K.B.; Schlesier, C.; Junghans, K.; Zhang, Y.; Olmstead, M.M.; Balch, A.L.; Dunsch, L.; Popov, A.A. Endohedral fullerene with μ3-carbido ligand and titanium-carbon double bond stabilized inside a carbon cage. *Nat. Commun.* **2014**, *5*, 3568. [CrossRef] [PubMed]
12. Krause, M.; Ziegs, F.; Popov, A.A.; Dunsch, L. Entrapped bonded hydrogen in a fullerene: The five-atom cluster Sc_3CH in C_{80}. *Chem. Phys. Chem.* **2007**, *8*, 537–540. [CrossRef] [PubMed]
13. Wang, T.S.; Feng, L.; Wu, J.Y.; Xu, W.; Xiang, J.F.; Tan, K.; Ma, Y.H.; Zheng, J.P.; Jiang, L.; Lu, X.; et al. Planar quinary cluster inside a fullerene cage: Synthesis and structural characterizations of $Sc_3NC@C_{80}$-I_h. *J. Am. Chem. Soc.* **2010**, *132*, 16362–16364. [CrossRef]
14. Stevenson, S.; Mackey, M.A.; Stuart, M.A.; Phillips, J.P.; Easterling, M.L.; Chancellor, C.J.; Olmstead, M.M.; Balch, A.L. A distorted tetrahedral metal oxide cluster inside an icosahedral carbon cage. Synthesis, isolation, and structural characterization of $Sc_4(\mu_3\text{-}O)_2@I_h$-$C_{80}$. *J. Am. Chem. Soc.* **2008**, *130*, 11844–11845. [CrossRef] [PubMed]
15. Dunsch, L.; Yang, S.F.; Zhang, L.; Svitova, A.; Oswald, S.; Popov, A.A. Metal sulfide in a C_{82} fullerene cage: A new form of endohedral clusterfullerenes. *J. Am. Chem. Soc.* **2010**, *132*, 5413–5421. [CrossRef] [PubMed]
16. Yang, S.F.; Chen, C.B.; Liu, F.P.; Xie, Y.P.; Li, F.Y.; Jiao, M.Z.; Suzuki, M.; Wei, T.; Wang, S.; Chen, Z.F.; et al. An improbable monometallic cluster entrapped in a popular fullerene cage: $YCN@C_s(6)$-C_{82}. *Sci. Rep.* **2013**, *3*, 1487. [CrossRef] [PubMed]
17. Chaur, M.N.; Valencia, R.; Rodríguez-Fortea, A.; Poblet, J.M.; Echegoyen, L. Trimetallic nitride endohedral fullerenes: Experimental and theoretical evidence for the $M_3N^{6+}@C_{2n}{}^{6-}$ model. *Angew. Chem. Int. Ed.* **2009**, *48*, 1425–1428. [CrossRef] [PubMed]
18. Rodríguez-Fortea, A.; Balch, A.L.; Poblet, J.M. Endohedral metallofullerenes: A unique host–guest association. *Chem. Soc. Rev.* **2011**, *40*, 3551–3563. [CrossRef]
19. Lu, X.; Bao, L.P.; Akasaka, T.; Nagase, S. Recent progress in the chemistry of endohedral metallofullerenes. *Chem. Commun.* **2014**, *50*, 14701–14715. [CrossRef]
20. Bao, L.P.; Peng, P.; Lu, X. Bonding inside and outside Fullerene Cages. *Acc. Chem. Res.* **2018**, *51*, 810–815. [CrossRef]
21. Yamada, M.; Tanabe, Y.; Dang, J.S.; Sato, S.; Mizorogi, N.; Hachiya, M.; Suzuki, M.; Abe, T.; Kurihara, H.; Maeda, Y.; et al. D_{2d}(23)-C_{84} versus $Sc_2C_2@D_{2d}$(23)-C_{84}: Impact of Endohedral Sc_2C_2 Doping on Chemical Reactivity in the Photolysis of Diazirine. *J. Am. Chem. Soc.* **2016**, *138*, 16523–16532. [CrossRef] [PubMed]
22. Akasaka, T.; Kato, T.; Kobayashi, K.; Nagase, S.; Yamamoto, K.; Funasaka, H.; Takahashi, T. Exohedral adducts of $La@C_{82}$. *Nature* **1995**, *374*, 600–601. [CrossRef]

23. Yamada, M.; Nakahodo, T.; Wakahara, T.; Tsuchiya, T.; Maeda, Y.; Akasaka, T.; Kako, M.; Yoza, K.; Horn, E.; Mizorogi, N.; et al. Positional control of encapsulated atoms inside a fullerene cage by exohedral addition. *J. Am. Chem. Soc.* **2005**, *127*, 14570–14571. [CrossRef] [PubMed]
24. Maeda, Y.; Matsunaga, Y.; Wakahara, T.; Takahashi, S.; Tsuchiya, T.; Ishitsuka, M.O.; Hasegawa, T.; Akasaka, T.; Liu, M.T.H.; Kokura, K.; et al. Isolation and characterization of a carbene derivative of La@C_{82}. *J. Am. Chem. Soc.* **2004**, *126*, 6858–6859. [CrossRef] [PubMed]
25. Maeda, Y.; Miyashita, J.; Hasegawa, T.; Wakahara, T.; Tsuchiya, T.; Nakahodo, T.; Akasaka, T.; Mizorogi, N.; Kobayashi, K.; Nagase, S.; et al. Reversible and regioselective reaction of La@C_{82} with cyclopentadiene. *J. Am. Chem. Soc.* **2005**, *127*, 12190–12191. [CrossRef] [PubMed]
26. Iezzi, E.B.; Duchamp, J.C.; Harich, K.; Glass, T.E.; Lee, H.M.; Olmstead, M.M.; Balch, A.L.; Dorn, H.C. A Symmetric Derivative of the Trimetallic Nitride Endohedral Metallofullerene, Sc_3N@C_{80}. *J. Am. Chem. Soc.* **2002**, *124*, 524–525. [CrossRef] [PubMed]
27. Yamada, M.; Wakahara, T.; Nakahodo, T.; Tsuchiya, T.; Maeda, Y.; Akasaka, T.; Yoza, K.; Horn, E.; Mizorogi, N.; Nagase, S. Synthesis and structural characterization of endohedral pyrrolidinodimetallofullerene: La_2@$C_{80}(CH_2)_2$NTrt. *J. Am. Chem. Soc.* **2006**, *128*, 1402–1403. [CrossRef] [PubMed]
28. Cardona, C.M.; Kitaygorodskiy, A.; Echegoyen, L. Trimetallic nitride endohedral metallofullerenes: Reactivity dictated by the encapsulated metal cluster. *J. Am. Chem. Soc.* **2005**, *127*, 10448–10453. [CrossRef] [PubMed]
29. Feng, L.; Nakahodo, T.; Wakahara, T.; Tsuchiya, T.; Maeda, Y.; Akasaka, T.; Kato, T.; Horn, E.; Yoza, K.; Mizorogi, N.; et al. A singly bonded derivative of endohedral metallofullerene: La@$C_{82}CBr(COOC_2H_5)_2$. *J. Am. Chem. Soc.* **2005**, *127*, 17136–17137. [CrossRef]
30. Lukoyanova, O.; Cardona, C.M.; Rivera, J.; Lugo-Morales, L.Z.; Chancellor, C.J.; Olmstead, M.M.; Rodríguez-Fortea, A.; Poblet, J.M.; Balch, A.L.; Echegoyen, L. "Open Rather than Closed" malonate methano-fullerene derivatives. The formation of methanofulleroid adducts of Y_3N@C_{80}. *J. Am. Chem. Soc.* **2007**, *129*, 10423–10430. [CrossRef]
31. Bao, L.P.; Chen, M.Q.; Pan, C.W.; Yamaguchi, T.; Kato, T.; Olmstead, M.M.; Balch, A.L.; Akasaka, T.; Lu, X. Crystallographic Evidence for Direct Metal–Metal Bonding in a Stable Open-Shell La_2@I_h-C_{80} Derivative. *Angew. Chem. Int. Ed.* **2016**, *128*, 4314–4318. [CrossRef]
32. Jin, F.; Tamm, N.B.; Troyanov, S.I.; Yang, S.F. Steering the Geometry of Butterfly-Shaped Dimetal Carbide Cluster within a Carbon Cage via Trifluoromethylation of Y_2C_2@C_{82}(6). *J. Am. Chem. Soc.* **2018**, *140*, 3496–3499. [CrossRef] [PubMed]
33. Iiduka, Y.; Wakahara, T.; Nakahodo, T.; Tsuchiya, T.; Sakuraba, A.; Maeda, Y.; Akasaka, T.; Yoza, K.; Horn, E.; Kato, T.; et al. Structural determination of metallofullerene Sc_3C_{82} revisited: a surprising finding. *J. Am. Chem. Soc.* **2005**, *127*, 12500–12501. [CrossRef]
34. Kurihara, H.; Lu, X.; Iiduka, Y.; Mizorogi, N.; Slanina, Z.; Tsuchiya, T.; Akasaka, T.; Nagase, S. Sc2C2@C80 Rather than Sc2@C82: Templated Formation of Unexpected C2v(5)-C80 and Temperature-Dependent Dynamic Motion of Internal Sc2C2 Cluster. *J. Am. Chem. Soc.* **2011**, *133*, 2382–2385.
35. Jin, P.; Li, Y.; Magagula, S.; Chen, Z.F. Exohedral functionalization of endohedral metallofullerenes: Interplay between inside and outside. *Coordin. Chem. Rev.* **2019**, *388*, 406–439. [CrossRef]
36. Akasaka, T.; Kato, T.; Nagase, S.; Kobayashi, K.; Yamamoto, K.; Funasaka, H.; Takahashi, T. Chemical derivatization of endohedral metallofullerene La@C_{82} with digermirane. *Tetrahedron* **1996**, *52*, 5015–5020. [CrossRef]
37. Yamada, M.; Feng, L.; Wakahara, T.; Tsuchiya, T.; Maeda, Y.; Lian, Y.; Kako, M.; Akasaka, T.; Kato, T.; Kobayashi, K.; et al. Synthesis and characterization of exohedrally silylated M@C82 (M = Y and La). *J. Phys. Chem. B* **2005**, *109*, 6049–6051.
38. Wakahara, T.; Yamada, M.; Takahashi, S.; Nakahodo, T.; Tsuchiya, T.; Maeda, Y.; Akasaka, T.; Kako, M.; Yoza, K.; Horn, E. Two-dimensional hopping motion of encapsulated La atoms in silylated La_2@C_{80}. *Chem. Commun.* **2007**, 2680–2682. [CrossRef]
39. Yamada, M.; Wakahara, T.; Tsuchiya, T.; Maeda, Y.; Kako, M.; Akasaka, T.; Yoza, K.; Horn, E.; Mizorogi, N.; Nagase, S. Location of the metal atoms in Ce_2@C_{78} and its bis-silylated derivative. *Chem. Commun.* **2008**, 558–560. [CrossRef]
40. Wakahara, T.; Iiduka, Y.; Ikenaga, O.; Nakahodo, T.; Sakuraba, A.; Tsuchiya, T.; Maeda, Y.; Kako, M.; Akasaka, T.; Yoza, K. Characterization of the bis-silylated endofullerene Sc_3N@C_{80}. *J. Am. Chem. Soc.* **2006**, *128*, 9919–9925. [CrossRef]
41. Kako, M.; Miyabe, M.; Sato, K.; Suzuki, M.; Mizorogi, N.; Wang, W.-W.; Yamada, M.; Maeda, Y.; Olmstead, M.M.; Balch, A.L.; et al. Preparation, structural determination, and characterization of electronic properties of bis-silylated and bis-germylated Lu_3N@I_h-C_{80}. *Chem. Eur. J.* **2015**, *21*, 16411–16420. [CrossRef] [PubMed]
42. Kako, M.; Nagase, S.; Akasaka, T. Functionalization of endohedral metallofullerenes with reactive silicon and germanium compounds. *Molecules* **2017**, *22*, 1179. [CrossRef] [PubMed]
43. Kako, M.; Miyabe, K.; Fukazawa, S.; Kanzawa, S.; Yasui, M.; Yamada, M.; Maeda, Y.; Slanina, Z.; Uhlík, F.; Adamowicz, L.; et al. Photoreactions of Sc_3N@C_{80} with disilirane, silirane, and digermirane: A photochemical method to separate I_h and D_{5h} Isomers. *Photochem* **2022**, *2*, 122–137. [CrossRef]
44. Cao, B.P.; Wakahara, T.; Maeda, Y.; Han, A.H.; Akasaka, T.; Kato, T.; Kobayashi, K.; Nagase, S. Lanthanum Endohedral Metallofulleropyrrolidines: Synthesis, Isolation, and EPR Characterization. *Chem. Eur. J.* **2004**, *10*, 716–720. [CrossRef] [PubMed]
45. Yamada, M.; Okamura, M.; Sato, S.; Someya, C.I.; Mizorogi, N.; Tsuchiya, T.; Akasaka, T.; Kato, T.; Nagase, S. Two Regioisomers of Endohedral Pyrrolidinodimetallofullerenes M_2@I_h-$C_{80}(CH_2)_2$NTrt (M=La, Ce; Trt=trityl): Control of Metal Atom Positions by Addition Positions. *Chem.- Eur. J.* **2009**, *15*, 10533–10542. [CrossRef] [PubMed]
46. Cai, T.; Ge, Z.X.; Iezzi, E.B.; Glass, T.E.; Harich, K.; Gibson, H.W.; Dorn, H.C. Synthesis and characterization of the first trimetallic nitride templated pyrrolidino endohedral metallofullerenes. *Chem. Commun.* **2005**, 3594–3596. [CrossRef] [PubMed]

47. Wang, T.; Wu, J.; Xu, W.; Xiang, J.; Lu, X.; Li, B.; Jiang, L.; Shu, C.; Wang, C. Spin Divergence Induced by Exohedral Modification: ESR Study of $Sc_3C_2@C_{80}$ Fulleropyrrolidine. *Angew. Chem. Int. Ed.* **2010**, *49*, 1830–1833. [CrossRef]
48. Yu, B.; Shen, W.Q.; Yang, L.; Liu, Y.C.; Pan, C.W.; Cong, H.L.; Jin, P.; Lu, X. Regioselective synthesis, crystallographic characterization, and electrochemical properties of pyrazole- and pyrrole-ring-fused derivatives of $Y_2@C_{3v}(8)$-C_{82}. *Chem. Eur. J.* **2020**, *26*, 2464–2469. [CrossRef]
49. Chen, M.Q.; Guan, R.N.; Li, B.; Yang, L.; Niu, C.; Jin, P.; Wang, G.W.; Yang, S.F. Anomalous *cis*-conformation regioselectivity of heterocycle-fused $Sc_3N@D_{3h}$-C_{78} derivatives. *Angew. Chem. Int. Ed.* **2021**, *60*, 7880–7886. [CrossRef]
50. Miao, C.B.; Tian, Z.Y.; Ruan, X.J.; Sun, X.Q.; Yang, H.T. Reaction of [60]fullerene with poxides under photo-irradiation: Synthesis of C_{60}-fused tetrahydrofuran derivatives. *Heterocycles* **2011**, *83*, 1615–1620. [CrossRef]
51. Wang, G.W.; Wu, P.; Yang, H.T.; Miao, C.B.; Xu, Y. Novel cycloaddition reaction of [60] fullerene with carbonyl ylides generated from epoxides. *J. Org. Chem.* **2006**, *71*, 4346–4348. [CrossRef] [PubMed]
52. Aroua, S.; Garcia-Borràs, M.; Bölter, M.F.; Osuna, S.; Yamakoshi, Y. Endohedral metal-induced regioselective formation of bis-Prato adduct of $Y_3N@I_h$-C_{80} and $Gd_3N@I_h$-C_{80}. *J. Am. Chem. Soc.* **2015**, *137*, 58–61. [CrossRef] [PubMed]
53. Cerón, M.R.; Izquierdo, M.; Garcia-Borràs, M.; Lee, S.S.; Stevenson, S.; Osuna, S.; Echegoyen, L. Bis-1,3-dipolar cycloadditions on endohedral fullerenes $M_3N@I_h$-C_{80} (M = Sc, Lu): Remarkable endohedral-cluster regiochemical control. *J. Am. Chem. Soc.* **2015**, *137*, 11775–11782. [CrossRef] [PubMed]
54. Semivrazhskaya, O.; Romero-Rivera, A.; Aroua, S.; Troyanov, S.I.; Garcia-Borràs, M.; Stevenson, S.; Osuna, S.; Yamakoshi, Y. Structures of $Gd_3N@C_{80}$ Prato bis-adducts: Crystal structure, thermal isomerization, and computational study. *J. Am. Chem. Soc.* **2019**, *141*, 10988–10993. [CrossRef] [PubMed]
55. Semivrazhskaya, O.; Aroua, S.; Yulikov, M.; Romero-Rivera, A.; Stevenson, S.; Garcia-Borràs, M.; Osuna, S.; Yamakoshi, Y. Regioselective synthesis and characterization of tris- and tetra-Prato adducts of $M_3N@C_{80}$ (M = Y, Gd). *J. Am. Chem. Soc.* **2020**, *142*, 12954–12965. [CrossRef] [PubMed]
56. Bolskar, R.D.; Benedetto, A.F.; Husebo, L.O.; Price, R.E.; Jackson, E.F.; Wallace, S.; Wilson, L.J.; Alford, J.M. First soluble $M@C_{60}$ derivatives provide enhanced access to metallofullerenes and permit in vivo evaluation of $Gd@C_{60}[C(COOH)_2]_{10}$ as a MRI contrast agent. *J. Am. Chem. Soc.* **2003**, *125*, 5471–5478. [CrossRef] [PubMed]
57. Feng, L.; Wakahara, T.; Nakahodo, T.; Tsuchiya, T.; Piao, Q.; Maeda, Y.; Lian, Y.F.; Akasaka, T.; Horn, E.; Yoza, K.; et al. The bingel monoadducts of $La@C_{82}$: Synthesis, characterization, and electrochemistry. *Chem. Eur. J.* **2006**, *12*, 5578–5586. [CrossRef]
58. Shen, W.Q.; Yang, L.; Li, B.; Jin, P.; Yu, B.; Cong, H.L.; Akasaka, T.; Lu, X. Metal-encapsulation induces a highly regioselective Bingel–Hirsch reaction of the labile $Y@C_s(6)$-C_{82}. *Chem. Commun.* **2020**, *56*, 14357–14360. [CrossRef]
59. Li, F.F.; Rodriguez-Fortea, A.; Poblet, J.M.; Echegoyen, L. Reactivity of Metallic Nitride Endohedral Metallofullerene Anions: Electrochemical Synthesis of a $Lu_3N@I_h$-C_{80} Derivative. *J. Am. Chem. Soc.* **2011**, *133*, 2760–2765. [CrossRef]
60. Chaur, M.N.; Melin, F.; Elliott, B.; Athans, A.J.; Walker, K.; Holloway, B.C.; Echegoyen, L. The influence of cage size on the reactivity of trimetallic nitride metallofullerenes: A mono- and bis-methanoadduct of $Gd_3N@C_{80}$ and a monoadduct of $Gd_3N@C_{84}$. *Chem. Commun.* **2008**, 2665–2667. [CrossRef]
61. Wang, S.; Huang, J.; Gao, C.L.; Jin, F.; Li, Q.X.; Xie, S.Y.; Yang, S.F. Singly bonded monoadduct rather than methanofullerene: Manipulating the addition pattern of trimetallic nitride clusterfullerene through one endohedral metal atom substitution. *Chem. Eur. J.* **2016**, *22*, 8309–8315. [CrossRef] [PubMed]
62. Hu, Y.J.; Solé-Daura, A.; Yao, Y.R.; Liu, X.C.; Liu, S.J.; Yu, A.; Peng, P.; Poblet, J.M.; Rodríguez-Fortea, A.; Echegoyen, L.; et al. Chemical reactions of cationic metallofullerenes: An alternative route for exohedral functionalization. *Chem. Eur. J.* **2020**, *26*, 1748–1753. [CrossRef] [PubMed]
63. Yamada, M.; Someya, C.; Wakahara, T.; Tsuchiya, T.; Maeda, Y.; Akasaka, T.; Yoza, K.; Horn, E.; Liu, M.T.H.; Mizorogi, N.; et al. Metal Atoms Collinear with the Spiro Carbon of 6,6-Open Adducts, $M_2@C_{80}$(Ad) (M = La and Ce, Ad = Adamantylidene). *J. Am. Chem. Soc.* **2008**, *130*, 1171–1176. [CrossRef] [PubMed]
64. Iiduka, Y.; Wakahara, T.; Nakajima, K.; Nakahodo, T.; Tsuchiya, T.; Maeda, Y.; Akasaka, T.; Yoza, K.; Liu, M.T.H.; Mizorogi, N.; et al. Experimental and Theoretical Studies of the Scandium Carbide Endohedral Metallofullerene $Sc_2C_2@C_{82}$ and Its Carbene Derivative. *Angew. Chem. Int. Ed.* **2007**, *46*, 5562–5564. [CrossRef] [PubMed]
65. Yamada, M.; Abe, T.; Saito, C.; Yamazaki, T.; Sato, S.; Mizorogi, N.; Slanina, Z.; Uhlík, F.; Suzuki, M.; Maeda, Y.; et al. Adamantylidene Addition to $M_3N@I_h$-C_{80} (M=Sc, Lu) and $Sc_3N@D_{5h}$-C_{80}: Synthesis and Crystallographic Characterization of the [5,6]-Open and [6,6]-Open Adducts. *Chem. Eur. J.* **2017**, *23*, 6552–6561. [CrossRef] [PubMed]
66. Chen, M.Q.; Bao, L.P.; Ai, M.; Shen, W.Q.; Lu, X. $Sc_3N@I_h$-C_{80} as a novel lewis acid to trap abnormal N-heterocyclic carbene unprecedented formation of a singly bonded [6, 6, 6]-adduct. *Chem. Sci.* **2016**, *7*, 2331–2334. [CrossRef]
67. Chen, M.Q.; Shen, W.Q.; Peng, P.; Bao, L.P.; Zhao, S.S.; Xie, Y.P.; Jin, P.; Fang, H.Y.; Li, F.F.; Lu, X. Evidence of oxygen activation in the reaction between an N-heterocyclic carbene and $M_3N@I_h(7)$-C_{80}: An unexpected method of steric hindrance release. *J. Org. Chem.* **2017**, *82*, 3500–3505. [CrossRef] [PubMed]
68. Shen, W.Q.; Yang, L.; Wu, Y.; Bao, L.P.; Li, Y.; Jin, P.; Fang, H.Y.; Xie, Y.P.; Lu, X. Reactions between N-heterocyclic carbene and lutetium-metallofullerenes: High regioselectivity directed by electronic effect in addition to steric hindrance. *J. Org. Chem.* **2019**, *84*, 606–612. [CrossRef]

69. Liu, X.Y.; Li, B.; Yang, W.; Yao, Y.R.; Yang, L.; Zhuang, J.X.; Li, X.M.; Jin, P.; Chen, N. Synthesis and characterization of carbene derivatives of Th@C_{3v}(8)-C_{82} and U@C_{2v}(9)-C_{82}: Exceptional chemical properties induced by strong actinide-carbon cage interaction. *Chem. Sci.* **2021**, *12*, 2488–2497. [CrossRef]
70. Chen, M.Q.; Zhao, Y.X.; Jin, F.; Li, M.Y.; Guan, R.N.; Xin, J.P.; Yao, Y.R.; Zhao, X.; Wang, G.W.; Zhang, Q.Y.; et al. Decisive role of non-rare earth metals in high-regioselectivity addition of μ_3-carbido clusterfullerene. *Inorg. Chem. Front.* **2022**, *9*, 5688–5696. [CrossRef]
71. Nikawa, H.; Kikuchi, T.; Wakahara, T.; Nakahodo, T.; Tsuchiya, T.; Rahman, G.M.A.; Akasaka, T.; Maeda, Y.; Yoza, K.; Horn, E.; et al. Missing Metallofullerene La@C_{74}. *J. Am. Chem. Soc.* **2005**, *127*, 9684–9685. [CrossRef] [PubMed]
72. Shu, C.Y.; Cai, T.; Xu, L.S.; Zuo, T.M.; Reid, J.; Harich, K.; Dorn, H.C.; Gibson, H.W. Manganese(III)-Catalyzed Free Radical Reactions on Trimetallic Nitride Endohedral Metallofullerenes. *J. Am. Chem. Soc.* **2007**, *129*, 15710–15717. [CrossRef] [PubMed]
73. Jin, F.; Wang, S.; Tamm, N.B.; Yang, S.F.; Troyanov, S.I. Synthesis, Isolation and Trifluoromethylation of Two Isomers of C_{84}-based Monometallic Cyanide Clusterfullerenes: Interplay between the Endohedral Cluster with the Exohedral Addend. *Angew. Chem. Int. Ed.* **2017**, *56*, 11990–11994. [CrossRef] [PubMed]
74. Liu, F.P.; Velkos, G.; Krylov, D.S.; Spree, L.; Zalibera, M.; Ray, R.; Samoylova1, N.A.; Chen, C.H.; Rosenkranz, M.; Schiemenz1, S.; et al. Air-stable redox-active nanomagnets with lanthanide spins radical-bridged by a metal–metal bond. *Nat. Commun.* **2019**, *10*, 571. [CrossRef] [PubMed]
75. Han, X.Y.; Xin, J.P.; Yao, Y.R.; Liang, Z.H.; Qiu, Y.F.; Chen, M.Q.; Yang, S.F. Capturing the long-sought Dy@C_{2v}(5)-C_{80} via benzyl radical stabilization. *Nanomaterials* **2022**, *12*, 3291. [CrossRef] [PubMed]
76. Xu, D.; Jiang, Y.H.; Wang, Y.Y.; Zhou, T.H.; Shi, Z.J.; Omachi, H.; Shinohara, H.; Sun, B.Y.; Wang, Z.Y. Turning on the near-infrared photoluminescence of erbium metallofullerenes by covalent modification. *Inorg. Chem.* **2019**, *58*, 14325–14330. [CrossRef] [PubMed]
77. Li, J.; Yu, P.Y.; Lai, P.; Zou, J.J.; Liu, Z.; Yi, X.G.; Wang, W.; Pan, C.W. Regioselective Radical Reaction of Monometallofullerene Y@C2v(9)-C82 With N-arylbenzamidine Mediated by Silver Carbonate. *Front. Chem.* **2020**, *8*, 593602. [CrossRef] [PubMed]
78. Wang, Y.F.; Velkos, G.; Israel, N.J.; Rosenkranz, M.; Büchner, B.; Liu, F.P.; Popov, A.A. Electrophilic trifluoromethylation of dimetallofullerene anions en route to air-stable single-molecule magnets with high blocking temperature of magnetization. *J. Am. Chem. Soc.* **2021**, *143*, 18139–18149. [CrossRef]
79. Chen, C.-H.; Yeh, W.Y.; Liu, Y.H.; Lee, G.H. [(μ-H)$_3$Re$_3$(CO)$_9$(η^2, η^2, η^2-Sc$_2$C$_2$@C_{3v}(8)-C_{82})]: Face-capping cluster complex of an endohedral fullerene. *Angew. Chem. Int. Ed.* **2012**, *51*, 3046–13049. [CrossRef]
80. Xie, Y.P.; Pan, C.W.; Bao, L.P.; Slanina, Z.; Akasaka, T.; Lu, X. Regioselective coordination of Re$_2$(CO)$_{10}$ to Y@C_{2v}(9)-C_{82}: An unprecedented η1 complex stabilized by intramolecular electron transfer. *Organometallics* **2019**, *38*, 2259–2263. [CrossRef]
81. Bao, L.P.; Yu, P.Y.; Li, Y.; Pan, C.W.; Shen, W.Q.; Jin, P.; Liang, S.Q.; Lu, X. Highly regioselective complexation of tungsten with Eu@C_{82}/Eu@C_{84}: Interplay between endohedral and exohedral metallic units induced by electron transfer. *Chem. Sci.* **2019**, *10*, 4945–4950. [CrossRef] [PubMed]
82. Hu, Y.J.; Yao, Y.R.; Liu, X.C.; Yu, A.; Xie, X.M.; Abella, L.; Rodríguez-Fortea, A.; Poblet, J.M.; Akasaka, T.; Peng, P.; et al. Unexpected formation of 1,2- and 1,4-bismethoxyl Sc$_3$N@I_h-C_{80} derivatives via regioselective anion addition: An unambiguous structural identification and mechanism study. *Chem. Sci.* **2021**, *12*, 8123–8130. [CrossRef] [PubMed]
83. Niu, C.; Liu, Z.; Chen, M.Q.; Yang, S.F.; Wang, G.W. Unexpected formation of pyrazoline-fused metallofullerenes from the multicomponent cascade reaction of Sc$_3$N@I_h-C_{80} with tetrazines, water, and oxygen. *Org. Lett.* **2022**, *24*, 3493–3498. [CrossRef] [PubMed]
84. Kurihara, H.; Iiduka, Y.; Rubin, Y.; Waelchli, M.; Mizorogi, N.; Slanina, Z.; Tsuchiya, T.; Nagase, S.; Akasaka, T. Unexpected formation of a Sc$_3$C$_2$@C_{80} bisfulleroid derivative. *J. Am. Chem. Soc.* **2012**, *134*, 4092–4095. [CrossRef] [PubMed]
85. Li, Y.B.; Emge, T.J.; Moreno-Vicente, A.; Kopcha, W.P.; Sun, Y.; Mansoor, I.F.; Lipke, M.C.; Hall, G.S.; Poblet, J.M.; Rodríguez-Fortea, A.; et al. Unexpected formation of metallofulleroids from multicomponent reactions, with crystallographic and computational studies of the cluster motion. *Angew. Chem. Int. Ed.* **2021**, *60*, 25269–25273. [CrossRef] [PubMed]
86. Pykhova, A.D.; Semivrazhskaya, O.O.; Samoylova, N.A.; Rybalchenko, A.V.; Rosenkranz, M.; Ioffe, I.N.; Popov, A.A.; Goryunkov, A.A. Addition of CF$_2$ group to endohedral fullerene Sc$_3$N@I_h-C_{80}. *Dalton Trans.* **2020**, *49*, 9137–9147. [CrossRef] [PubMed]
87. Pykhova, A.D.; Olesya, O. Semivrazhskaya, O.O.; Samoylova, N.A.; Popov, A.A.; Ioffe, I.N.; Goryunkov, A.A. Regioselective CF$_2$ functionalization of Sc$_3$N@D_{3h}(5)-C_{78}. *Dalton Trans.* **2022**, *51*, 1182–1190. [CrossRef]